Science Advances

Supplementary Materials for

Measles virus nucleo- and phosphoproteins form liquid-like phase-separated compartments that promote nucleocapsid assembly

Serafima Guseva, Sigrid Milles, Malene Ringkjøbing Jensen, Nicola Salvi, Jean-Philippe Kleman, Damien Maurin, Rob W. H. Ruigrok*, Martin Blackledge*

*Corresponding author. Email: martin.blackledge@ibs.fr (M.B.); rob.ruigrok@ibs.fr (R.W.H.R.)

The PDF file includes:

Table S1
Figs. S1 to S8
Legends for movies S1 and S2
Data S1

Other Supplementary Material for this manuscript includes the following:

(available at advances.sciencemag.org/cgi/content/full/6/14/eaaz7095/DC1)
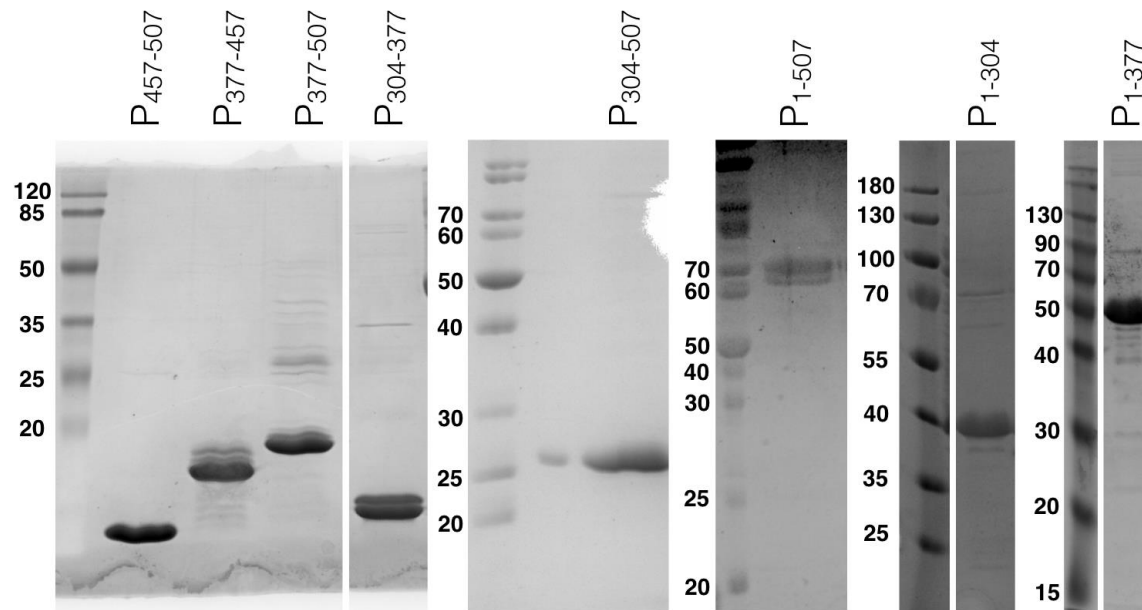
Movie S1 and S2

Table S1

Ptot (μM)	Ntot (μM)	P$_D$ (μM)	N$_D$ (μM)	ratio
75	7,5	43,23	5,77	0,13
75	15	54,60	8,64	0,16
75	37,5	72,3	13,49	0,19
75	75	75	26,74	0,36

Calculated ratio of [N]/[P] in liquid droplets as determined from NMR (see main text)

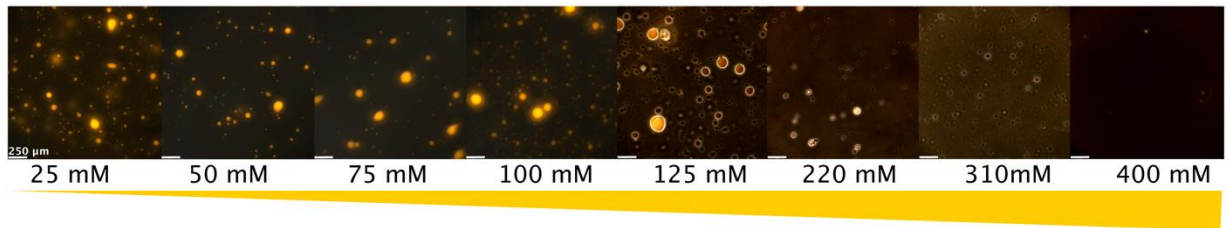**Fig. S1** SDS-PAGE (15%) with Coomassie staining of purified truncated constructs of P and P$_{1-507}$.

Fig. S2

Fluorescent images overlaid with DIC show the salt dependence of LLPS formation. $P_{50}N_{525}$ (100 µM, 1% fluorescently labelled) and $P_{304-507}$ (100 µM) were used, NaCl concentration in buffer was increased linearly from 25 mM to 400 mM.
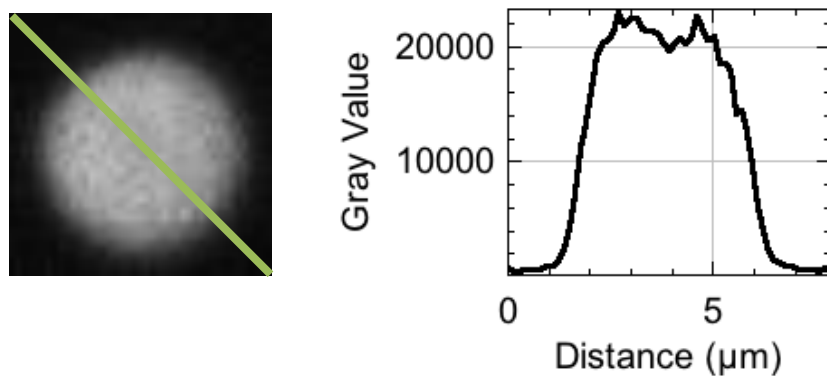
Fig. S3

Fluorescence image of a droplet formed by $P_{50}N_{525}$ (25 µM, 0.04% labelled) and $P_{304-507}$ (50 µM) and its intensity profile represent homogeneous protein distribution within the droplet.
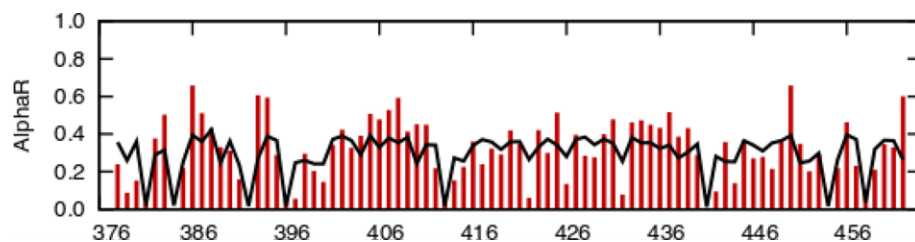

Fig. S4. Secondary structural propensity of P$_{LOOP}$

Population of α-helical secondary structure of P_{LOOP} showing 15% and 10% difference between the statistical coil ensemble (black line) and the selected ensemble using ASTEROIDS (red bars) for regions 405-411 and 433-438 respectively.
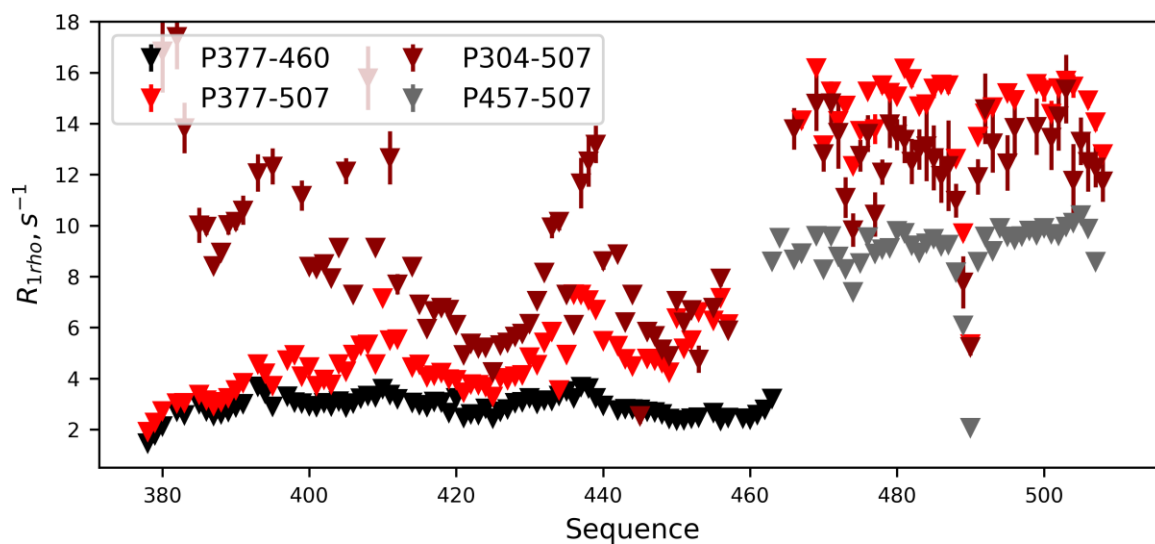
Fig. S5. Dynamic behaviour of P$_{LOOP}$

^{15}N R$_{1\rho}$ of P$_{LOOP}$ (concentration 500µM), P$_{XD}$ (concentration 500µM), P$_{377-507}$ (concentration 100 µM) and P$_{304-507}$ (concentration 100 µM) measured at 25ºC, ^{1}H frequency of 850MHz. Information about the tetramerization domain is not available as resonances for this region are not observable under these experimental conditions.
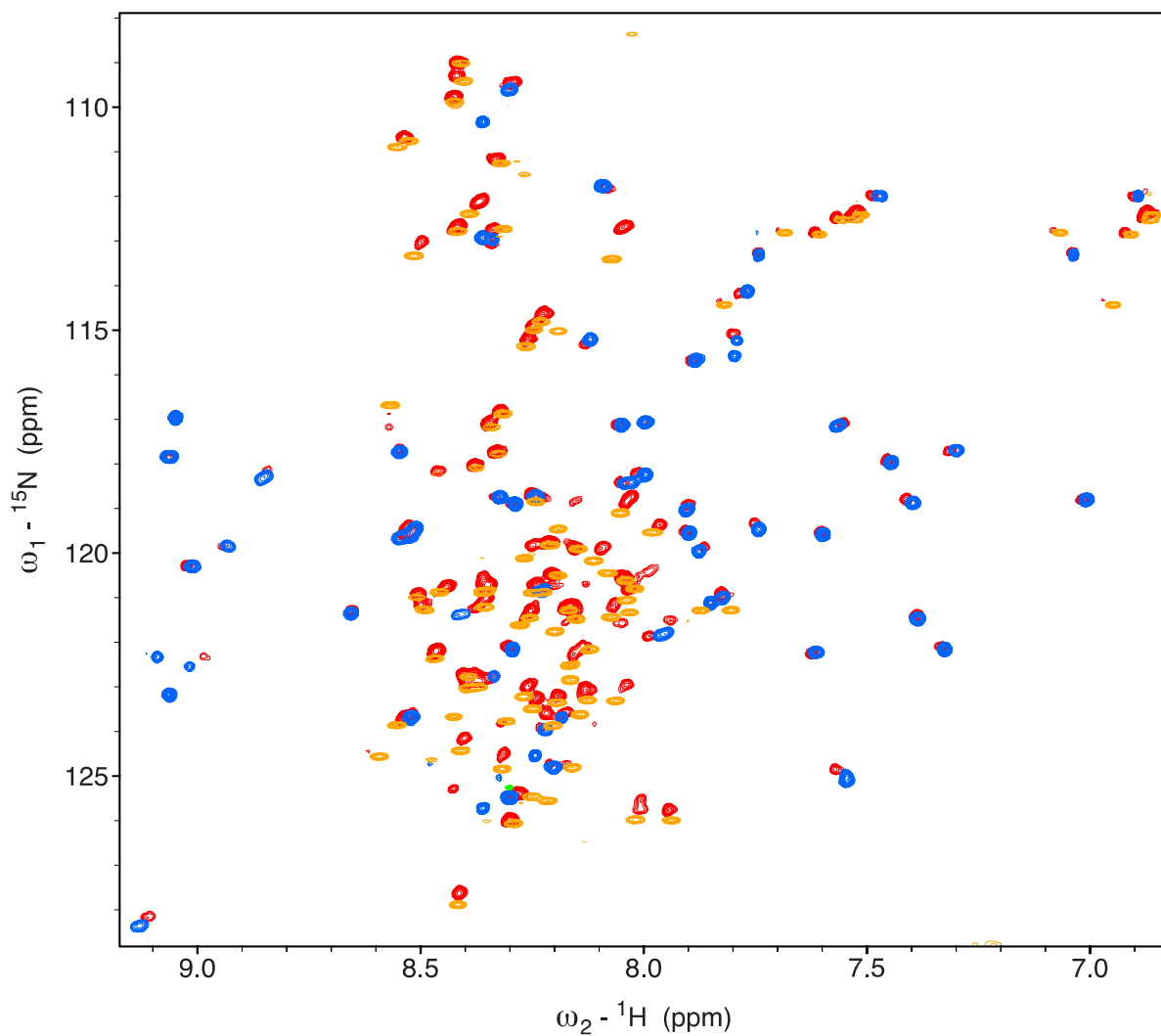
Fig. S6 P_{LOOP} remains unfolded in the context of phase separating protein constructs

^{1}H-^{15}N HSQC spectrum of P$_{304-507}$ (red) (298K, phosphate buffer, 150mM salt and pH 6.0, 240 μM, 200 increments, 20 scans) overlapped with P$_{LOOP}$ (orange, 100 μM, 200 increments, 20 scans) and P$_{XD}$ (blue, 100 μM, 400 increments, 16 scans), all spectra were recorded at ^{1}H frequency of 700 MHz.

Fig. S7 Sequence analysis of P_{LOOP}

Measles virus phosphoprotein homologs were found using The Basic Local Alignment Search Tool (BLAST) from the Swiss-Prot database, non-truncated sequences were chosen for further analysis (110 sequences) and visualised using https://weblogo.berkeley.edu for residues 377-460.
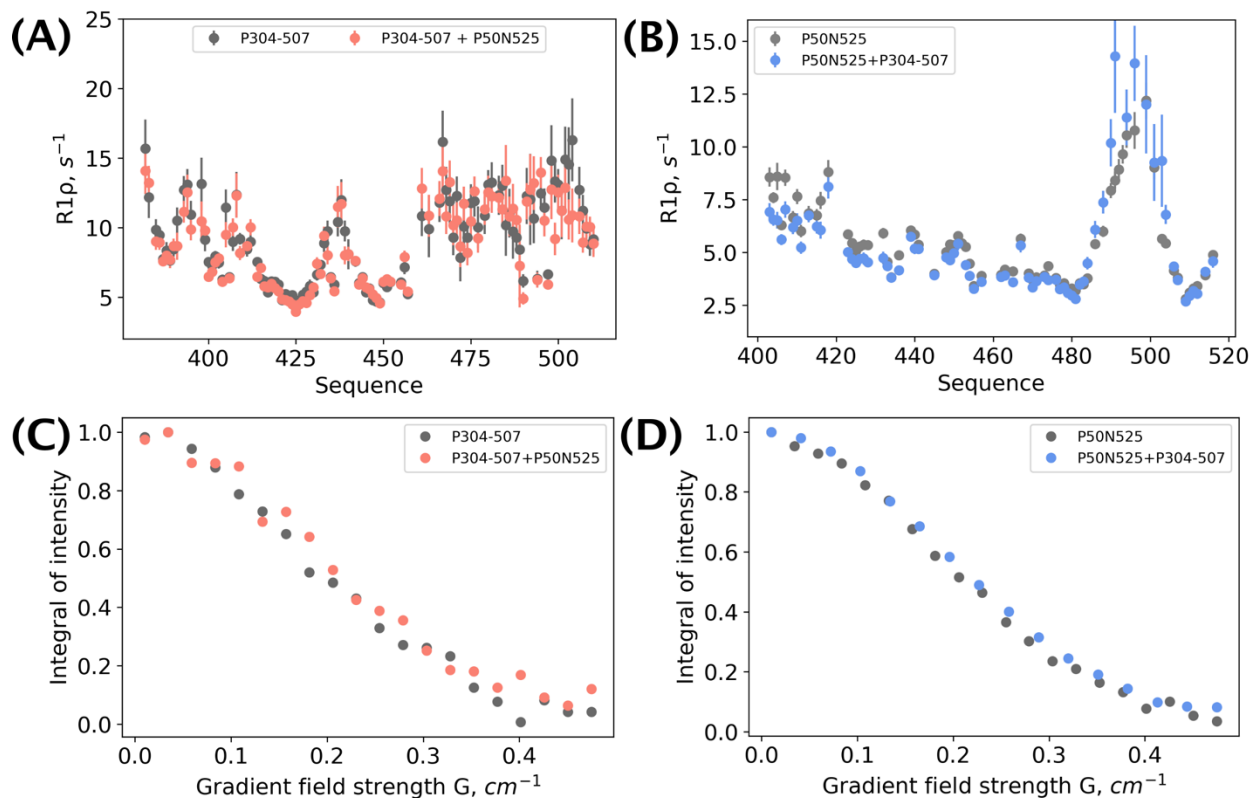
Fig. S8 NMR signals of both $P_{50}N_{525}$ and $P_{304-507}$ at phase separating conditions exhibit similar characteristics as for the same proteins in the dilute phase. $R_{1\rho}$ profiles at 25ºC 700 MHz for (A) $P_{304-507}$ alone (100 μM, grey) and with $P_{50}N_{525}$ (10 μM, salmon pink); (B) $P_{50}N_{525}$ alone (100 μM, grey) and with $P_{304-507}$ (10 μM, blue) measured at 25ºC 850 MHz. Translational diffusion for (C) $P_{304-507}$ alone (75 μM, grey) and with $P_{50}N_{525}$ (7.5 μM salmon pink); (D) $P_{50}N_{525}$ alone (75 μM, grey) and with $P_{304-507}$ (37.5 μM, blue).

Movie S1.

Droplets formed by $P_{50}N_{525}$ (10 µM) and $P_{304-507}$ (100 µM) highlighting examples of fusion upon touching within several seconds. The video speed is accelerated by a factor of 2. Scale bar is 24 µM.

Movie S2.

Fluorescence microscopy images showing RNA diffusing into droplets pre-formed by mixing $P_{50}N_{525}$ (20 µM) and $P_{304-507}$ (80 µM). Concentration of RNA was 200 µM (with 10% labelled RNA-FAM). RNA was added on one side of the coverslip and spontaneously diffused in the sample, the time gap between images is 2 seconds. Scale bar is 240 µm.

Data S1. Chemical shift assignment of P_{LOOP}

```
Phosphate buffer 50 mM, pH 6.0
NaCl 150 mM
DTT 2 mM
298K
```

	N	H	CO	CA
378	110.825	8.547	173.598	45.1
379	120.357	8.075	176.122	55.6725
380	124.46	8.585	–	51.967
381	–	–	176.947	63.866
382	116.607	8.56	174.73	53.2185
383	121.187	7.868	174.841	51.963
384	–	–	177.501	63.791
385	112.628	8.307	174.57	62.221
386	125.898	7.931	177.289	52.525
387	120.012	8.261	176.157	54.3155
388	119.453	7.975	175.915	62.016
389	124.335	8.404	176.204	56.325
390	122.421	8.158	175.570	60.769
391	123.769	8.544	175.475	50.978
392	–	–	176.839	63.799
393	118.767	8.237	176.206	54.675
394	121.208	7.801	176.957	54.8565
395	123.226	8.057	174.311	54.424
396	–	–	176.76	62.97
397	121.527	8.27	176.414	61.1525
398	125.462	8.209	176.664	61.0285
399	113.247	8.508	–	45.27
400	120.772	8.211	175.369	56.342
401	121.18	8.484	176.527	54.325
402	116.791	8.308	174.497	59.009
403	110.679	8.52	–	45.643
404	120.718	8.015	176.277	56.2955
405	124.762	8.311	178.064	52.741
406	121.392	8.145	177.412	55.471
407	123.543	8.137	178.092	52.8755
408	119.372	8.186	176.854	56.8525
409	120.959	8.032	176.299	62.8285
410	124.725	8.154	177.172	55.149
411	122.084	8.115	176.176	56.105
412	123.781	8.196	174.404	54.235
413	–	–	176.956	63.005
414	120.81	8.238	176.162	62.334
415	127.802	8.409	177.804	52.554
416	115.276	8.258	174.830	58.399
417	122.887	8.355	176.364	56.477
418	121.129	8.35	176.079	56.0555
419	123.42	8.248	177.496	55.307
420	120.78	8.343	176.515	56.2045

421	109.802	8.418	174.26	45.393
422	119.745	8.205	176.704	55.594
423	114.736	8.223	174.476	61.8445
424	120.912	8.501	175.683	53.414
425	108.94	8.403	174.228	53.7865
426	120.423	8.187	176.710	56.241
427	114.908	8.237	174.672	61.821
428	118.005	8.367	174.731	58.2235
429	118.119	8.451	174.817	58.525
430	122.69	8.385	177.03	56.721
431	109.341	8.398	174.29	45.52
432	119.83	8.141	176.09	55.967
433	123.153	8.263	177.379	55.401
434	122.777	8.158	177.498	55.2965
435	121.688	8.193	176.799	56.7215
436	120.792	8.358	176.455	57.0605
437	120.096	8.107	175.580	57.8815
438	121.372	8.069	175.441	55.6295
439	123.226	8.121	176.98	55.143
440	123.287	8.188	174.287	54.016
441	–	–	176.959	63.176
442	121.382	8.249	176.902	61.241
443	112.707	8.41	173.911	53.479
444	121.208	8.16	176.546	56.162
445	122.953	8.381	176.632	56.408
446	122.294	8.461	176.3	47.0785
447	117.099	8.336	174.536	58.301
448	117.699	8.32	174.152	58.23
449	125.997	8.287	177.706	52.516
450	119.024	8.046	176.698	62.557
451	112.3	8.384	173.454	53.363
452	120.551	8.035	175.076	57.809
453	125.899	8.014	173.687	59.259
454	–	–	176.44	62.95
455	120.785	8.452	176.577	54.386
456	113.322	8.066	174.994	61.418
457	111.182	8.317	–	44.798
458	–	–	177.126	63.412
459	123.569	8.419	177.996	52.58
460	114.92	8.183	174.749	58.295